Prediction of churning losses in an industrial gear box with spiral bevel gears using the smoothed particle hydrodynamic method

B. Legrady[1] · M. Taesch[1] · G. Tschirschnitz[1] · C. F. Mieth[2]

Abstract

Sufficient and reliable lubrication is vital to avoid gear and bearing failure under various operating conditions in gearboxes. In conservative approaches, this requirement is fulfilled by an oil oversupply that can come with excessive load-independent power losses. Current methods for estimating churning losses do not provide sufficiently accurate predictions to optimize the oversupply, motivating the investigation of alternative novel methodologies.

The scope of this work is to analyze the oil distribution and churning losses of a spiral bevel gear transmission using the novel meshless particle method, smoothed particle hydrodynamics (SPH), and to identify the largest loss contributors. Experimental investigations are carried out at a bevel gear test rig (KRPS) of the Chair of Machine Elements at Dresden University of Technology for a bevel gear pair under 1 kNm nominal load. These measurements provide validation data for load-dependent and -independent power losses at pinion rotational speeds of 1200–1800 rpm for different turning directions and filling heights. Both loss contributions follow a linear trend with rotational speed. Changing the turning direction so that oil is directly dragged into the gear interlocking region resulted in a load-dependent and -independent loss increase. Computational fluid dynamics simulations are conducted with the SPH-Software developed by dive solutions GmbH. Analyzing the fluid field of the simulation at a low speed in a cold start situation shows good agreement with flow patterns of the experiment when surface tension models are included. To reproduce the qualitative trends of the experiments, simulations of the region of the interlocking bevel gears are conducted. Using these simulations, a further study on the gear geometry identified a difference of up to 30% in churning loses using decreased gear scales compared to using the same scales as in the experiment. When the bearings are considered in the simulation model, the churning losses of the experiment are correctly reproduced. A post-processing algorithm capable of evaluating the local churning loss of each component is developed. Thereby, the pinion with its shaft and the associated tapered roller element bearings are identified as the largest churning loss contributors.

✉ B. Legrady
legrady@dive-solutions.de

1   dive solutions GmbH, Bismarckstraße 10–12, 10625 Berlin, Germany

2   Institut für Maschinenelemente und Maschinenkonstruktion, Technische Universität Dresden, Helmholtzstraße 10, 01069 Dresden, Germany

Simulation der Planschverluste in einem spiralverzahnten Industriekegelradgetriebe mithilfe der Smoothed Particle Hydrodynamics Methode

Zusammenfassung

Um Zahnrad- und Lagerausfälle unter verschiedenen Betriebsbedingungen in Getrieben zu vermeiden, ist eine zuverlässige Schmierung unerlässlich. In konservativen Ansätzen wird diese Anforderung durch einen Ölüberschuss erfüllt, der mit übermäßigen lastunabhängigen Leistungsverlusten einhergehen kann. Standardmethoden zur Abschätzung der Planschverluste liefern keine ausreichend genauen Vorhersagen zur Optimierung der Ölversorgung, womit neuartige Simulationstechniken benötigt werden.

In dieser Untersuchung wird die Ölverteilung und die Planschverluste eines spiralverzahnten Kegelradgetriebes mithilfe der gitterfreien Methode Smoothed Particle Hydrodynamics (SPH) analysiert sowie die Verlustbeiträge der einzelnen Bauteile klassifiziert. Experimentelle Untersuchungen werden an einem Kegelradprüfstand (KRPS) der Professur für Maschinenelemente der Technischen Universität Dresden für ein Kegelradpaar unter 1 kNm Nennlast durchgeführt. Diese Messungen liefern Validierungsdaten für lastabhängige und -unabhängige Verlustleistungen bei Ritzeldrehzahlen von 1200–1800 U/min für verschiedene Drehrichtungen und Füllhöhen. Die experimentell bestimmten Verlustanteile folgen in Abhängigkeit der Drehzahl einem linearen Trend im Untersuchungsbereich. Eine Änderung der Drehrichtung, sodass das Öl direkt in den Verzahnungseingriff gezogen wird, führte zu einer Zunahme der lastabhängigen sowie -unabhängigen Verluste.

Die Strömungssimulationen werden mit der von dive solutions GmbH entwickelten SPH-Software durchgeführt. Die Analyse des Fluidfeldes der Simulation bei einer niedrigen Geschwindigkeit im Kaltstartszenario zeigt eine gute Übereinstimmung mit der Ölverteilung des Experiments, wenn zusätzlich ein physikalisches Modell der Oberflächenspannung einbezogen wird. Um die qualitativen Trends der Experimente zu reproduzieren, werden Simulationen des Bereichs der ineinandergreifenden Kegelräder durchgeführt. In einer weiteren simulativen Untersuchung der Zahnradgeometrie bei verkleinerten Zahnrändern wird eine Unterschätzung der Planschverluste von bis zu 30 % im Vergleich zur Verwendung der gleichen Skalen wie im Experiment festgestellt. Wenn die Lager im Simulationsmodell berücksichtigt werden, werden die Planschverluste des Experiments korrekt reproduziert. Es wird eine Postprocessing-Routine vorgestellt, die in der Lage ist, die lokale Planschverlustverteilung aller Komponenten auszuwerten. Dabei werden das Ritzel mit seiner Welle und die zugehörigen Kegelrollenlager als die größten Planschverlustquellen identifiziert.

1 Introduction

Mechanical engineering faces enormous challenges regarding energy efficiency, raw material consumption and environmental friendliness. The industry is constantly forced to develop new and innovative products or optimize their existing portfolio to comply with increasingly strict regulations regarding fuel consumption and emission. As of now, not only electrified engines and hybrid solutions but also hydrogen or e-fueled concepts thrive. Regardless of the final solution, drive train components are always required to deliver the power generated by an engine to the road surface. Current designs already manage to convert up to 97–99.5% of the generated mechanical input power to usable output power [1]. Nevertheless, maximizing the efficiency of gearboxes even further has a great potential, as this implies less heat dissipation for constant power. With that, the components that fulfil cooling tasks can be designed more compact. Less oil is required to decrease friction between the contacting gears and to absorb the dissipated heat from the drive train components. The lubricant itself is a resistance for the rotating parts. Emerging losses become more prominent with increasing rotational speed and decreasing

load—a typical situation for an automotive transmission at its top gear ratio [2].

Power losses within a gearbox are classified according to their component or origin, that is gears P_{LG}, bearings P_{LB}, seals, P_{LS}, and other parts or auxiliary components, P_{LX}, like clutches and electric pumps. Losses of the individual components are further divided into load-dependent, index L, and load-independent losses, sometimes referred to as spin or no-load losses, index 0. Following the notation of Niemann and Winter [3], the power losses may be written as

$$P_L = P_{LG} + P_{LG0} + P_{LB} + P_{LB0} + P_{LS} + P_{LX}. \tag{1}$$

Sophisticated models and methods exist to determine load-dependent losses. In contrary, accurate prediction of load-independent losses require an accurate prediction of the interaction between lubricant and fluid which is a priori unknown as all components interact with the lubricant in a coupled manner. The load-independent losses are grouped by their physical origin. Churning, index C, arises due to the parts moving the inertia of the oil by pressure and viscous forces acting from the fluid towards the wheel. Squeezing, index S, covers losses that are generated by the rapid

volume changes in the periodically opening and closing meshing zone. Windage, index W, covers losses due to air resistance. This yields the general formulation of load-independent losses in a passive lubricated gearbox

$$P_{L0} = P_C + P_S + P_W. \tag{2}$$

It has been commonly observed that losses due to air resistance are negligible for circumferential speeds below 20 m/s [4, 5].

Although experimental research on the topic of gear power losses has been conducted since mid of the 20th century [6] and extensive studies have been made in the following decades [7, 8], no general concept has been developed to accurately determine power losses in a complete gearboxes. The difficulty stems from the fact that the fluid flow within gearboxes is inherently complex. This is caused by the complexly shaped bodies churning through the lubricant-air mixture. The fluid phenomena for bevel gears are inherently more dynamic than cylindrical gears due to their exposed three-dimensional shape and mounting position. Only little research on bevel gear churning losses has been conducted. Experimental studies on single rotating bevel gears made by Laruelle et al. [4] propose a formulation for the churning torque over filling height, gear radius and rotational speed for different fluid regimes. Quiban et al. [9] updated these formulations and highlighted the phenomena of decreasing churning torques for dynamically varying filling heights. A broad range of tests for different hypoid gears, rotational speed, oils, attitudes, single and meshing gears have been conducted by Jeon [10]. This study provides quantitative measurements for a specific gearbox. Therefore, his findings cannot be applied to arbitrary bevel-geared transmissions.

With the advent of high-performance computing and the progress of computational fluid dynamic (CFD) methods, simulations of the motion of the fluid within a gearbox became feasible [11, 12]. Subsequently, it was demonstrated that CFD is capable of accurately reproducing the fluid dynamics observed in experiments [13]. The investigations of the last decades are based on traditional CFD approaches that utilize a grid-based Eulerian technique. These methods are established but have to cope with major difficulties: With increasing complexity, that is more moving geometries, narrow gaps and large geometry curvature, generating a sophisticated computational grid becomes difficult [14, 15]. Tracking the complex phase interface between air and oil requires a sufficiently fine mesh and the transient deformation of the domain with its moving parts requires to adapt the grid over time. These demands raise the computational effort drastically. A variety of mesh and geometry handling techniques are employed to cope with this matter. A summary is given in Concli and Gorla [16] and Concli

et al. [15]. However, these methods have been proven to reliably predict churning losses [12, 13, 15].

Smoothed Particle Hydrodynamics (SPH) is a Lagrangian technique that avoids these difficulties. Here, particles of distinct fluid types represent individual phases. In comparison to the Eulerian approach, no computational grid is required, and the unique particle type implicitly reconstructs the phase interface. Apart from the native handling of multi-phase and free surfaces flows, SPH has also proven to provide computational advantages for gearbox simulations. Keller et al. [17] as well as Maier et al. [18] conducted SPH simulations 20–25 times faster than a Eulerian simulation of the same problem. These aspects indicate the significant potential of the SPH method in the field of transmission CFD. Being meshfree, it simplifies the time-consuming geometry preparation and the simulation itself, by making typical procedures such as remeshing or gear-scaling obsolete. Although overall fluid flow was reproduced accurately [19–22] this method has not yet proven to replicate the measured churning losses [20]. The origin of this discrepancy is not yet found. Contrary to the previous papers, the utilized SPH solver imposes the boundary-particle interaction by segments instead of boundary particles. This approach enables to reproduce quantitatively accurate churning losses and the capability to qualitative capture trends with filling height, rotational speed and direction accordingly, which is shown in this paper. Moving particle semi-implicit (MPS) characterizes another Lagrangian CFD method. Both MPS and SPH are very similar in their numerical approach as shown in Soute-Iglesias et al. [23]. The churning loss determined by applying the MPS method on a high-speed railway system is qualitatively investigated in a similar study conducted by Deng et al. [24]. The results presented in [24] are derived from an implicit MPS solver that allows for larger time-steps than the explicit SPH solver in this paper. However, implicit solvers come with the disadvantage to solve the pressure Poisson equation by a computational costly matrix inversion.

2 Numerical approach

Fundamental to the SPH method is the spatially discrete representation of a continuum with so-called particles. These collocation points, which move along their trajectories, inherit the physical properties of the continuum.

A weighted interpolation at these points is used to determine its properties based on its distance from adjacent particles and their physical quantities. Here, the Wendland kernel of fifth order (Fig. 1) is used as weighting function. Using the derivative of the kernel, the SPH formalism al-
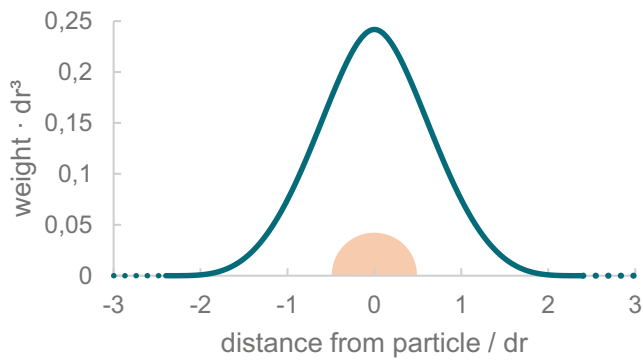
Fig. 1 1D visualization of the 3D Wendland kernel of fifth order (*solid line*). At the *dashed line*, the function is zero. The hemisphere indicates a particle at the position of the evaluation

lows for an approximation of spatial derivatives, which is crucial for solving partial differential equations numerically.

Often, liquids are considered incompressible, so the density remains constant. In the current work, however, a weakly compressible approach is utilized. This means that a small density change, less than 1%, is allowed. Instead of solving a Poisson equation to determine the pressure, an equation of state links the pressure directly to the density change.

The mathematical basis of fluid dynamics is derived using this preposition. Incompressibility is considered for the derivation of the momentum equation. Contrarily, the continuity equation is solved in its compressible form to account for the change in the density. Here, the equation of state proposed by Cole [25, 26] is used. This yields the governing equations for weakly compressible SPH in the Lagrangian formulation:

$$\begin{aligned}
\frac{d\boldsymbol{x}}{dt} &= \boldsymbol{v}, \\
\frac{d\rho}{dt} &= -\rho \nabla \cdot \boldsymbol{v}, \\
\frac{d\boldsymbol{v}}{dt} &= -\frac{1}{\rho} \nabla p + \frac{1}{\rho} \nabla \cdot \left(\mu \left(\nabla \otimes \boldsymbol{v} + (\nabla \otimes \boldsymbol{v})^T \right) \right) + \boldsymbol{g}, \\
p &= \frac{\rho_0 c_0^2}{\gamma} \left(\frac{\rho}{\rho_0} - 1 \right)^{\gamma} + p_0,
\end{aligned} \tag{3}$$

with position of the particles x, velocity v, time t, density ϱ, pressure p, dynamic viscosity μ, gravity g, background pressure p_0, artificial speed of sound c_0, reference density ϱ_0 and exponent γ, which is chosen as 7.0 for oil [26] and 1.4 for air [27, 28].

Equations 3 are discretized using the SPH formalism. The temporal derivates are discretized using a Runge-Kutta 4 scheme [29]. To improve numerical stability and the quality of the pressure field, an additional diffusive term is added to the continuity equation [30]. To improve the particle distribution, a particle shifting technique is applied [31]. This improves the interpolation quality of the scheme [32]. In this work, no turbulence model is utilized.

For the boundary representation, there are two major approaches:

- The boundaries are thickened with so-called dummy particles, that can be included in the regular particle interaction [25].
- Integral boundary conditions use a segment-based mesh representation of shapes [33].

In Sabrowski et al. [28], the different boundary condition approaches are discussed specifically for gearbox applications. In this work, a segment-based mesh representation is utilized to treat boundary conditions. This approach was chosen as it allows for a very accurate and native representation of Computer-Aided Design (CAD) geometries in the SPH method.

The calculation of churning losses is executed by means of pressure F_{pi} and viscous forces F_{vi} acting on the i-th rotating boundary triangle with area A_i and normal vector n_i as

$$\begin{aligned}
F_{pi} &= p_i A_i n_i, \\
F_{vi} &= \mu \left(\frac{\partial \boldsymbol{v}}{\partial \boldsymbol{x}} \right)_i A_i n_i.
\end{aligned} \tag{4}$$

The specific torque generated around the rotational axis of each component j is calculated as

$$T_j = \sum_i r_i \times \left(F_{pi} + F_{vi} \right), \tag{5}$$

with the lever r_i eventually leading to a formulation for the power P_j required to move the lubricant

$$P_j = \omega_j T_j. \tag{6}$$

Reorganizing the expressions leads to a local formulation of the power losses by means of viscous P_{vi} and pressure P_{pi} induced power losses

$$P_j = \sum_i \left(P_{pi} + P_{vi} \right), \tag{7}$$

which will be used to evaluate the power loss distribution for each component.

3 Experimental setup

The torque test bench "Kegelradprüfstand" (KRPS) at Dresden University of Technology (TUD) is used for this study. It consists of two slave and two test gearboxes of similar characteristics shown in Fig. 2. Test gearbox 2 is investigated in detail. The load torque is applied on the pinion side, torque is measured with an HBM torque transducer
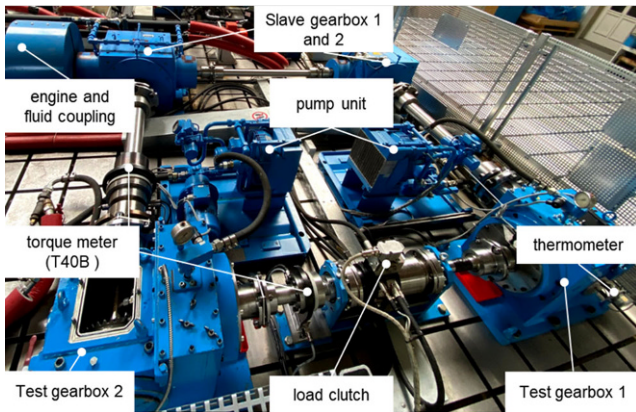
Fig. 2 Bevel gear torque test bench (KRPS) at Dresden University of Technology

Table 1 Oil properties of Mobilube HD 80W-90 for the investigated operating conditions
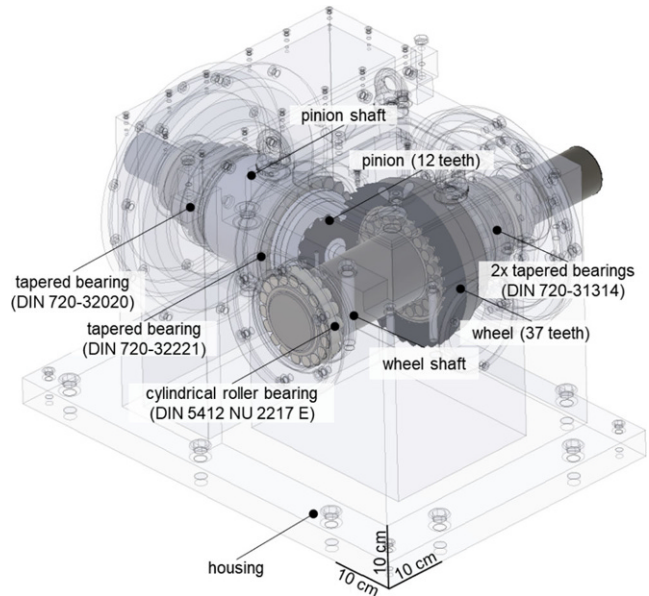
Temperature (°C)	Density (kg/m^3)	Kin. Viscosity (cSt)
26	894	310
60	875	53

Fig. 3 Geometry model of the test gearbox. Neither injection nor pumping system are included

of type T40B on the shaft of the pinion and as well as the wheel.

Temperature was measured at the bottom of the oil reservoir. A temperature of $60 \pm 2\,°C$ was ensured throughout all torque experiments. For the experiments, the oil Mobilube HD 80W-90 was used. The oil properties at the respective investigation temperatures are given in Table 1.

The test gearbox comprises a bevel gear stage of gear ratio 3.08. The pinion shaft is supported by two roller tapered bearings in X-mounting position, the wheel is supported by two smaller tapered bearings in O-mounting position and an additional cylindrical roller bearing. The digital model (Fig. 3) does not include an active lubrication system in between the pinion bearings and the meshing zone as well as the pumping system and pipes at the bottom of the reservoir. This system cannot be removed nor switched off. However, previous studies at the test rig have shown that the lubrication effectiveness of the injection system is negligible.

The average torque loss was measured for rotational speeds between 1200 to 1800 rpm, filling heights of 10, 45 and 85 mm below the centerlines and both turning directions. The gearbox of size $700 \times 500 \times 500$ mm contain almost 16 L oil at the highest filling level. The rotational speed was increased stepwise; this increase was followed by a stepwise decreasing measurement resulting in two torque readings that cover 15 s of measurement time each. The load-dependent and injection lubricated torque losses were subtracted by employing a minimum lubricated test run. The gears are engaged in a driving mode for all operating conditions. For all tests, a constant load of 1 kNm had to

be applied on the pinion side to avoid damage to the slave gearboxes due to gear hammering. The following tests have been conducted for both turning directions, that is inwards (IN) if oil is immediately dragged into the meshing zone and outwards (OUT) otherwise. The gear characteristics are given in Table 2.

For a visual comparison, the cold start situation (26 °C and 600 rpm) was captured by removing the top lid of the housing. The amount of aeration has been visually verified to be small after the test run.

The simulations are conducted as follows: After an initial settling time of 0.02 s, both gears linearly accelerate to full speed at 0.08 s. The movements of the bearings are simplified as static rotations with half the rotational speed of the corresponding shafts. The simulation finishes at 1.1 s. The churning loss results are averaged over the last four rotations of the wheel.

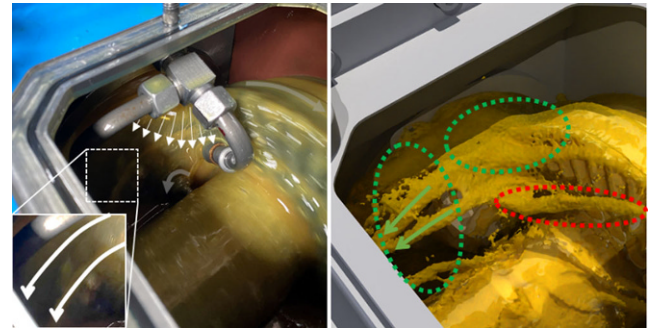## 4 Results

4.1 Oil distribution

The top lids of the test gearboxes were removed at the beginning of the test run to validate the capability of SPH to reproduce the oil distribution correctly. During the cold start, the oil viscosity is six times larger compared to the operating conditions at 60 °C. In addition, surface tension effects are more important due to an increased surface tension coefficient. For a rotational speed of 600 RPM, the oil fully covers the wheel. This behavior could only be re-

Table 2 Bevel gear pair characteristics

Parameter	Pinion	Wheel
Outside diameter d_0 (mm)	87.52	236.97
Mean pitch diameter d_p (mm)	66.96	206.46
Mean normal module m_{mn} (mm)	4.57	4.57
Number of teeth Z	12	37
Tooth width b (mm)	30	30
Tooth height h (mm)	10.28	10.28
Mean pitch angle δ (°)	17.97	72.03
Mean spiral angle β_m (°)	108.53	108.53
Generated normal pressure angle on drive side α_{nD} (°)	19.79	19.79
Handedness	Right	Left

Fig. 4 Experimental (*left*) and simulation (*right*) flow field for a cold start IN case at 600 rpm

produced in the simulations by including a surface tension model.

The IN case is visually investigated in test gearbox 2 for a filling height 10 mm below the axes (Fig. 4). Wheel and wheel shaft are coated with a thick oil film. The pinion is barely lubricated but not coated. Two large ligaments detach from the rear and front tip of the pinion shortly after the meshing zone. This behavior is stable. Oil partially flows to the largest diameter of the pinion at the rear tip due to centrifugal forces. The other share is squeezed towards the front tip of the pinion during the engagement process. Both effects lead to an accumulation of oil and eventually to the detachment in form of two ligaments. Both ligaments are

Fig. 5 Experimental (*left*) and simulation (*right*) flow field for a cold start OUT case at 600 rpm

also accurately captured by the corresponding SPH simulation.

The large, tapered bearing facing the meshing zone constantly pumps oil from the smaller inner diameter to the larger outer diameter. This results in a spray-alike wave that is ejected into the gear interaction area. The oil impinges at the injection system deflecting the jet away from the meshing zone. As a result, the jet injection is already ineffective at low RPM. The exact pumping effect of the tapered bearing is captured by the SPH simulation.

Contrary to the experiment, some oil ligaments periodically detach from the wheel in the simulation. This behavior starts in the meshing zone. It is assumed that the initial coating thickness from the emerging gear is too large due to the particle size of 1 mm. Overall, the coating thickness for both experiment and simulation appear similar.

For the OUT case (Fig. 5) with lower filling height, the wheel is still fully covered with oil, but only small oil droplets are formed on the shaft. This effect is caused by the surface tension minimizing the effective fluid at the surface. The coating is too thin to form larger oil accumulations that detach in either ligaments or droplets from the shaft. The simulation was able to reproduce this effect accurately. Another pattern is a large ligament emerging close to the pinion. The origin is not visible from footage but expected to be either connected to the pinion shaft or the tapered roller elements of the pinion. The SPH simulation contains a similar pattern that is caused by the roller elements. Again, some fluid detaches from the wheel in the simulation but not in the experiment.

4.2 Churning losses of the reduced system

Preliminary churning loss evaluations aim at the interaction of pinion and wheel exclusively. Only the gear interlocking with a 33% smaller reservoir is simulated. This measure does not yield any visual changes in oil distribution or deviations in the churning loss signal larger than 10%. For this
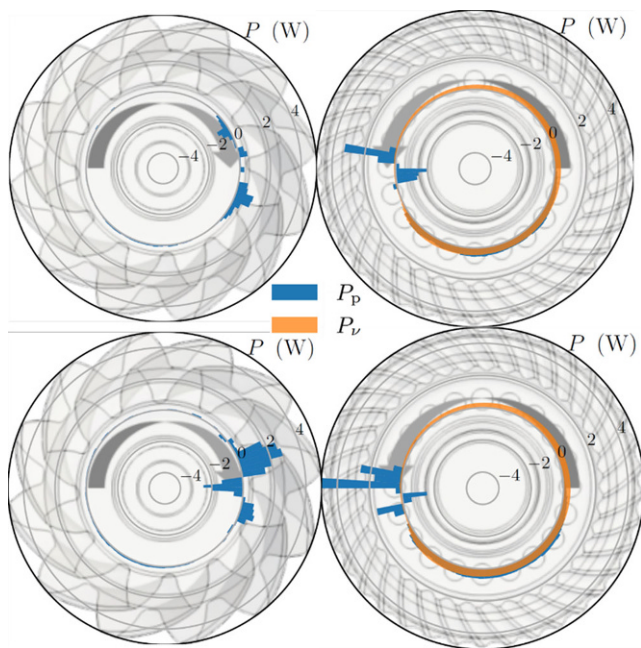
Fig. 6 Circumferential power loss distribution for the scaled (*top*) and unscaled (*bottom*) gear pair

setup, particles sizes have been varied between 0.5 to 5 mm resulting in negligible deviation for particles sizes below 1.5 mm. Simulating 7.2 l oil with this particle size results in an computational effort of 28 h on two Intel® Xeon® Gold 6248 @2.5 GHz without hyperthreading.

Moving the gears further apart or reducing the gear size are typical coping strategies to avoid grid topology singularities for mesh based CFD solvers [34]. The utilized SPH solver does not require these measures, which in turn allows to compare the results of scaled and unscaled gears. For this, the OUT case is employed for a filling height of 10 mm below the gear axes at 1600 rpm pinion speed. In the scaled case, the gears are scaled to 98% of their original radii. On average, the churning losses of the scaled gears are more than 30% smaller than the unscaled gears. Here, pressure induced losses decrease by 47% and viscous induced by 7%. Similarly, the wheel generated only 82% and the pinion 41% power losses compared to the unscaled gears.

A rough estimate for the validity of these deviations in the churning losses is made as follows: The gear surface velocity scales linearly with the radius. For an initial estimate, the wall shear stress is assumed to be linearly dependent on the boundary velocity for small radii changes. The effective surface area depends on the radius r and the pressure at the wall is proportional to the stagnation pressure that is $\frac{\rho}{2}v$š, thus, proportional to rš. Hence, viscous forces scale with rš and pressure induced forces with rş. The relation of force and torque is given by the lever r. Eventually, one derives a dependency of r^3 for the viscous induced power

losses and r^4 for the pressure induced losses as a rough estimate. This yields an expected reduction of 6% in viscous losses and 8% in pressure losses for the 98% scaling. With a measured decrease of 7% in viscous induced losses, the viscous loss reduction appears reasonable. Still, this estimation does not take fluid deflection in the meshing zone into account which is caused by pressure. In the scaled case, less resistance is generated in the interlocking zone of the gears, thus less fluid is squeezed outwards axially. This outcome is also visible at the circumferential loss distribution (Fig. 6). Pressure induced losses are mainly generated in the meshing zone of the gears. The pinion itself does not contribute noticeably since it digs itself free. This outcome has already been seen in the oil distribution for lower rpm. The viscous loss distribution looks similar but smaller for the scaled than the unscaled gears.

In the simulation using unscaled gears, the overall power losses are 84 W with 70 W being dissipated by the wheel and 14 W by the pinion. The pressure losses contribute to 49 W and the viscous losses to 35 W. It is apparent that viscous losses contribute significantly to the overall losses. This is caused by the high oil viscosity of over 50 cSt and the comparably small teeth. Cylindrical gears, in contrast, have the teeth at the outer diameter. This results in a full speed immersion with the full-face width, but for the spiral bevel gear the teeth can submerge and emerge with less oil resistance caused by their shape, hence leading to lower pressure losses.

4.3 Filling height and rotational speed parameter study

The oil filling height and rotational speed have been varied for the outward direction in experiments. The operating point at 1600 rpm and an oil level 10 mm below the axes serves as reference for the following comparison. The simulations are conducted in the reduced interaction domain and indicate the capabilities of SPH to predict the qualitative trends for important parameters. The relative change in churning losses over the filling height is given in Table 3 for the experiment and simulation. The percentage is given as reference to the operating conditions for the simulation and experiment, respectively.

The second experimental filling height has a large uncertainty as there was no possibility to measure the oil level directly but visually assuring that the pinion is not immersed. Similarly, the relative change in churning loss over rotational speed is given in Table 4. Simulation results show a similar tendency which proves the capacity of SPH to reproduce churning loss trends qualitatively.

Table 3 Relative changes of churning losses over filling height for the reduced system and the experiment in the OUT case

Filling height blow gear axes (m)	Simulation Losses (%)	Experiment Losses (%)
0.010	100	100
0.045	64	55
0.085	29	–

The respective value at 1600 rpm and 10 mm below the axes yields as reference

Table 4 Relative changes of churning losses over rotational speed for the reduced system and the experiment in the OUT case

Pinion (rpm)	Simulation Losses (%)	Experiment Losses (%)
1200	45	72
1400	–	84
1600	100	100
1800	106	116

The respective value at 1600 rpm and 10 mm below the axes yields as reference

4.4 Churning losses of the full gearbox

The difference in power losses from the filled and drained gearbox yields load-independent power losses. The results at the KRPS resulted in around 600 W for the inwards direction and 500 W for the outwards turning direction at 1600 rpm input speed and an oil level 10 mm below the gear axes. These values are almost one magnitude larger than the results presented in the reduced domain, thus the remaining pinion shaft and all bearings must generate substantial load-independent power losses. The particle size needed to be reduced to 1 mm to allow particles to enter the gap between pinion shaft and housing. Note that the flow in between the bearings is still under resolved with this particle diameter. A finer resolution would lead to more accurate and, thus, higher no-load losses in these regions. This, in turn, implies underestimated churning losses. Results per component and per physical loss origin are summarised in Table 5.

For both cases, the low speed bearings at the wheel shaft contribute to a negligible amount of churning losses. The smaller tapered bearing at the pinion shaft facing towards an additional reservoir has also a medium size share. In contrary, the large pinion bearing facing towards the gear interaction domain is responsible for almost one third of the load-independent power losses for both turning directions. Pressure losses in the bearing are a result of the pumping effect of the tapered bearings accelerating the oil from the smaller pinion shaft towards the outer diameter of the roller elements. Since these movements are simplified with a static rotation around the pinion shaft and the particle resolution is not sufficient to resolve viscous losses in between the roller elements properly, larger losses are ex-

Table 5 Component wise load-independent power losses for the IN and OUT case at 1600 rpm

Component	IN power losses (W)	OUT power losses (W)
Tapered bearings DIN 720-31314 (2x)	3	3
Cylindrical roller bearing D5412 NU 2217 E	7	6
Tapered bearing DIN 720-32020	26	23
Tapered bearing DIN 720-32221	112	101
Wheel	–12	79
Pinion	215	102
Pressure power losses (W)	192	165
Viscous power losses (W)	159	149
Total power losses (W)	351	314

pected with finer resolution. It is expected that applying the correct roller movements increases squeezing losses at the roller bearings. With this naïve rotation the flow is purely pushed. Preliminary estimations according the SKF Bearing Select (Version: 1.2.67) [35] proposed total bearing losses of up to 400 W depending on the exact mounting position which substantiates this hypothesis.

The major difference for both turning directions is seen (Fig. 7) in the loss contribution from pinion and wheel. The wheel power loss for the inward direction becomes even negative. Starting at the outward direction, the loss distribution for the wheel appears similar compared to the reduced system. The same holds for the pressure distribution of the pinion but the viscous losses are significantly larger. The reason for this behavior is visualized along the longitudinal coordinate of the pinion. The inner shaft is long and shrouded causing the oil to shear around the whole area. The circumferential distribution is slightly skewed around the rotational axis due to the dynamic change of the filling height and has the maximum below the pinion axis.

For the inward direction, the viscous loss distribution look similar along the longitudinal direction but skewed in the opposite direction along the rotational axis. Since both gears push fluid toward the engagement zone, the oil level is increased there and more area is wetted, thus, more viscous losses are generated. Moreover, the oil oversupply in the meshing zone account for substantial pressure induced losses. In this turning direction, the pinion mostly pushes the oil which, in turn, pushes the wheel. Why the total power loss of the wheel becomes negative for this turning direction is questionable and requires further investigation.
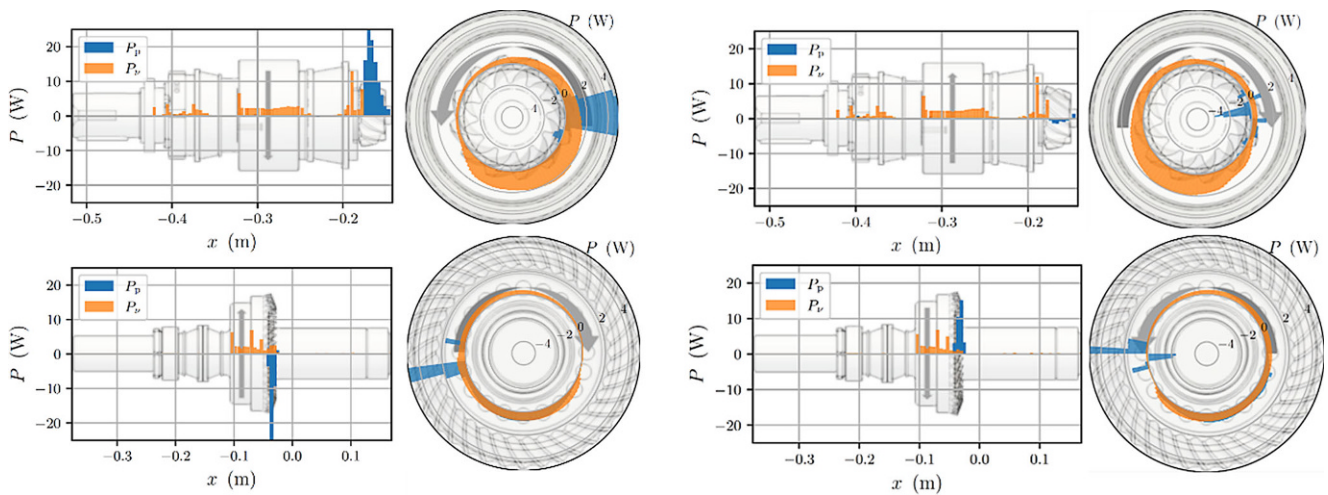
Fig. 7 Churning loss distribution for the OUT (*left*) and IN (*right*) case for the pinion (*top*) and the wheel (*bottom*) along and around their rotational axes

5 Conclusion and outlook

Understanding the lubrication flow in a bevel geared gearbox is the first step to comprehend the lubrication conditions in a transmission and take constructive measures to optimize these conditions. As the flow in bevel geared transmissions is inherently three-dimensional and complex, visual validation in experiments is not sufficient. The utilized SPH method provide a tool for easy and reliable industrial use to not only investigate these fluid patterns accurately but also derive reliable results for load-independent power losses.

The oil distribution in the SPH simulations is in very good agreement to the experiments and could be validated
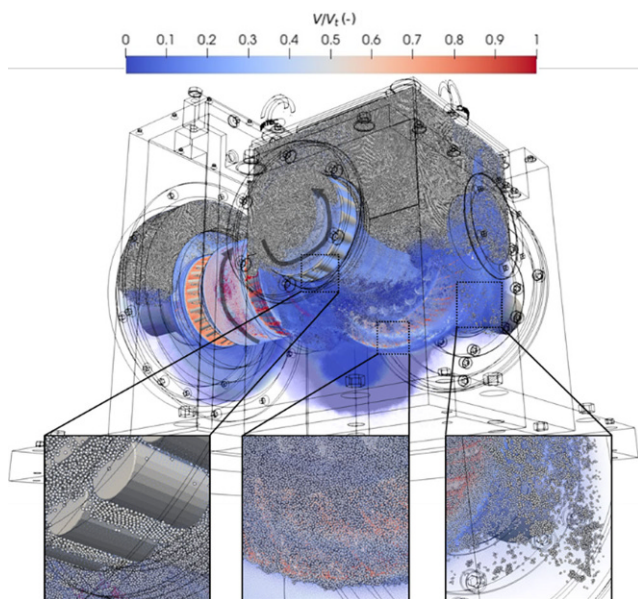
Fig. 8 Oil velocity distribution and highlighted air phase for the OUT case at 1600 rpm

visually. Load-independent power losses follow the expected trends for filling height, rotational speed and turning direction. Due to dominant no-load bearing losses which require higher resolutions, the absolute values are underestimated. The detected viscous spin losses are very large compared to previous studies and of the same magnitude as pressure losses. This is likely caused by the high viscous oil Mobilube HD 80W-90 at 60 °C and large areas at the churning shafts. Some uncertainties exist due to the effectiveness of the injection and suction system that is not included in the simulation. Additionally, it is unknown if the second reservoir might be filled over time by the pumping effect of the tapered bearing DIN 720-32020 which can account for substantial losses as well.

This proves that the SPH method is a potent tool to not only set up lubrication simulations within a few hours but also derive accurate results on the loss sources and their physical origin. In the case of a bevel gear pairing with several bearings, flow dynamics are highly complex and coupled which makes the usage of empirical formulas case dependent. This work provides a tool set with which not only oil lubrication but also churning losses and their local distribution can be investigated accurately. In addition, the robustness of SPH allows to use the geometries without further scaling, which results in higher accuracy for losses generated by the interaction of both gears. This claim is also substantiated using estimations.

A qualitative study in a reduced system on rotational speed and filling height shows that the SPH simulations follow the experimental trends. Investigating both turning directions experimentally revealed that dragging the oil into the meshing zone leads to larger losses. This is reproduced with the SPH simulation of the full system, and it was shown that not only the losses at the gears but also at the bearings increase in this turning direction.

Visual validation at low rpm and low temperature could prove that the injection system is partially deflected due to oil being ejected from tapered bearings which is correctly captured with the SPH method.

Utilizing the advantage of fast pre-processing and easy setup with accurate results in terms of oil distribution and churning losses renders the SPH method a potent tool for reduced product development cycles. The capability to react on important parameter like rotational speed, turning direction and filling height in reduced systems accordingly builds trust in secure A–B testing. This fact, in turn, extends the application range of the SPH method from pure lubrication simulations to power loss optimization as well. Using this tool in a cloud-based environment leverages the potential of SPH even further as various operating points can be investigated at the same time without depending on limited local hardware resources.

Further simulation investigation aim at the effects of multi-phase as seen in Fig. 8. Eventually, including the full injection system and refined particles around bearings will lead to high accuracy load-independent losses determination.

References

1. Schlecht B (2010) Maschinenelemente 2. Ing. Maschinenbau. Pearson, London
2. Polly J et al (2008) An experimental investigation of churning power losses of a gearbox. ATZ Worldw 110(4):36–43
3. Niemann G, Winter H (2003) Getriebe Allgemein, Zahnradgetriebe – Grundlagen, Stirnradgetriebe vol 2. Springer, Berlin, Heidelberg
4. Laruelle S et al (2017) Experimental investigations and analysis on churning losses of splash lubricated spiral bevel gears. Mech Ind 18(4):412
5. Petry-Johnson TT et al (2008) An experimental investigation of spur gear efficiency. J Mech Des 130(6):626011–6260110
6. Ohlendorf H /1958) Verlustleistung und Erwärmung von Stirnrädern. Dissertation, TH München
7. Terekhov A (1975) Hydraulic losses in gearboxes with oil immersion. Vestnik Mashinostroeniyanostroeniya 55(5):13–17
8. Mauz W (1987) Hydraulische Verluste von Stirnradgetrieben bei Umfangsgeschwindigkeiten bis 60 m/s. Dissertation, Stuttgart
9. Quiban R et al (2020) Churning losses of spiral bevel gears at high rotational speed. Proc Inst Mech Eng Part J Eng Tribol 234(2):36–43
10. Jeon SI (2010) Improving Efficiency in Drive Lines: an Experimental Study on Churning Losses in Hypoid Axle. PhD thesis, Imperial College
11. Arisawa H et al (2009) CFD simulation for reduction of oil churning losses and windage loss on aeroengine transmission gears. Proc ASME Turbo Expo 1:63–72
12. Gorla C et al (2013) Hydraulic losses of a gearbox: CFD analysis and experiments. Tribol Int 66:337–344
13. Mastrone MN et al (2020) Oil distribution and churning losses of gearboxes: experimental and numerical analysis. Tribol Int 151:106496
14. Liu H et al (2017) Determination of oil distribution and churning power loss of gearboxes by finite volume CFD method. Tribol Int 109:346–354
15. Concli F et al (2016) A new integrated approach for the prediction of the load independent power losses of gears: development of a mesh-handling algorithm to reduce the CFD simulation time. Adv Tribol 2016:1–8
16. Concli F, Gorla C (2016) Windage, churning and pocketing power losses of gears: different modeling approaches for different goals. Forsch Ingenieurwes 3–4:85–99
17. Keller M et al (2019) Smoothed particle hydrodynamics simulation of oil-jet gear interaction. J Tribol 141:1–7
18. Maier G et al (2019) nforderungen und Grenzen traditioneller FVM und neuer SPH-Ansätze zur Strömungssimulation in Fahrzeuggetrieben. NAFEMS Mag 52:42–52
19. Groenenboom PHL, Mettichi MZ, Gargouri Y (2015) Simulating oil flow for gearbox lubrication using smoothed particle hydrodynamics. Proc Int Conf Gears 8:1–10
20. Ji Z et al (2018) Numerical simulations of oil flow inside a gearbox by Smoothed Particle Hydrodynamics (SPH) method. Tribol Int 127:47–58
21. Liu H et al (2019) Numerical modelling of oil distribution and churning gear power losses of gearboxes by smoothed particle hydrodynamics. Proc Inst Mech Eng Part J J Eng Tribol 233(1):74–86
22. Menon M, Szewc K, Maurya V (2019) Multi-phase gearbox modelling using GPU-accelerated smoothed particle hydrodynamics method. In: Fluid applications and systems. Proceedings of the ASME-JSME-KSME 2019 8th Joint Fluids Engineering Conference, vol 3A, pp 1–10
23. Soute-Iglesias A et al (2013) On the consistency of MPS. Comput Phys Commun 184(3):732–745
24. Deng X et al (2020) Lubrication mechanism in gearbox of high-speed railway trains. J Adv Mech Des Syst Manuf. https://doi.org/10.1299/jamdsm.2020jamdsm0054
25. Adami S, Hu XY, Adams NA (2012) A generalized wall boundary condition for smoothed particle hydrodynamics. J Comput Phys 231:7057–7075
26. Cole HR (1948) Underwater explosions. Princeton University Press, Princeton
27. Grenier N et al (2009) A SPH multiphase formulation with a surface tension model applied to oil-water separation. In: Proceedings of the 4th SPHERIC International Workshop, Nantes, May 26–29, pp 22–29
28. Sabrowski P, Beck L, Wybranietz T (2019) Modern WCSPH in industrial multiphase application considering complex moving boundaries. In: Proceedings of the 14th SPHERIC International Workshop, Exeter, June 25–27, pp 266–273
29. Antuono M et al (2012) Numerical diffusive terms in weakly-compressible SPH schemes. Comput Phys Commun 183(12):2570–2580
30. Molteni D, Colagrossi A (2009) A simple procedure to improve the pressure evaluation in hydrodynamic context using the SPH. Comput Phys Commun 6:861–872
31. Lind SJ et al (2012) Incompressible smoothed particle hydrodynamics for free-surface flows: a generalised diffusion-based algorithm for stability and validations for impulsive flows and propagating waves. J Comput Phys 231:1499–1523
32. Oger G et al (2016) SPH accuracy improvement through the combination of a quasi-Lagrangian shifting transport velocity and consistent ALE formalisms. J Comput Phys 313:76–98
33. Chiron L et al (2019) Fast and accurate SPH modelling of 3D complex wall boundaries in viscous and non viscous flows. Comput Phys Commun 234:93–111
34. Liu H et al (2018) Detailed investigations on the oil flow in dip-lubricated gearboxes by the finite volume CFD method. Lubricants 6:47
35. SKF (2020) SKF bearing select (1.2.67). https://www.skf.com/group/support/engineering-tools/bearing-select. Accessed: 26.03.2021